J Arid Land (2024) 16(1): 110–130
https://doi.org/10.1007/s40333-024-0052-9

Science Press Springer-Verlag

Response of ecosystem carbon storage to land use change from 1985 to 2050 in the Ningxia Section of Yellow River Basin, China

LIN Yanmin[1,2], HU Zhirui[3], LI Wenhui[1,2], CHEN Haonan[1,2], WANG Fang[1,2*], NAN Xiongxiong[4], YANG Xuelong[5], ZHANG Wenjun[5]

[1] College of Geographical Sciences and Planning, Ningxia University, Yinchuan 750021, China;
[2] China-Arab Joint International Research Laboratory for Featured Resources and Environmental Governance in Arid Region, Yinchuan 750021, China;
[3] Ningxia Land Resources Surveying and Monitoring Institute, Yinchuan 750002, China;
[4] State Key Laboratory of Efficient Production of Forest Resources, Yinchuan 750002, China;
[5] Ningxia Lingwu Baijitan National Nature Reserve Administration, Yinchuan 751400, China

Abstract: Regional sustainable development necessitates a holistic understanding of spatiotemporal variations in ecosystem carbon storage (ECS), particularly in ecologically sensitive areas with arid and semi-arid climate. In this study, we calculated the ECS in the Ningxia Section of Yellow River Basin, China from 1985 to 2020 using the Integrated Valuation of Ecosystem Services and Tradeoffs (InVEST) model based on land use data. We further predicted the spatial distribution of ECS in 2050 under four land use scenarios: natural development scenario (NDS), ecological protection scenario (EPS), cultivated land protection scenario (CPS), and urban development scenario (UDS) using the patch-generating land use simulation (PLUS) model, and quantified the influences of natural and human factors on the spatial differentiation of ECS using the geographical detector (Geodetector). Results showed that the total ECS of the study area initially increased from 1985 until reaching a peak at 402.36×10^6 t in 2010, followed by a decreasing trend to 2050. The spatial distribution of ECS was characterized by high values in the eastern and southern parts of the study area, and low values in the western and northern parts. Between 1985 and 2020, land use changes occurred mainly through the expansion of cultivated land, woodland, and construction land at the expense of unused land. The total ECS in 2050 under different land use scenarios (ranked as EPS>CPS>NDS>UDS) would be lower than that in 2020. Nighttime light was the largest contributor to the spatial differentiation of ECS, with soil type and annual mean temperature being the major natural driving factors. Findings of this study could provide guidance on the ecological construction and high-quality development in arid and semi-arid areas.

Keywords: carbon storage; land use change; nighttime light; Integrated Valuation of Ecosystem Services and Tradeoffs (InVEST) model; patch-generating land use simulation (PLUS) model; geographical detector (Geodetector); Yellow River Basin

Citation: LIN Yanmin, HU Zhirui, LI Wenhui, CHEN Haonan, WANG Fang, NAN Xiongxiong, YANG Xuelong, ZHANG Wenjun. 2024. Response of ecosystem carbon storage to land use change from 1985 to 2050 in the Ningxia Section of Yellow River Basin, China. Journal of Arid Land, 16(1): 110–130. https://doi.org/10.1007/s40333-024-0052-9

1 Introduction

Ecosystem carbon storage (ECS), defined as the total amount of carbon stored in terrestrial

*Corresponding author: WANG Fang (E-mail: fangwang0820@nxu.edu.cn)
Received 2023-08-08; revised 2023-11-28; accepted 2023-12-08

ecosystems (He et al., 2016), is a crucial indicator of ecosystem functions. Since ECS is directly linked to ecosystem services (e.g., climate regulation) and productivity (Houghton, 2003; Zhao et al., 2019), enhancing carbon sequestration in terrestrial ecosystems is an essential strategy to increase the regional domestic product (Dong et al., 2019). Quantitative research on ECS could contribute to the sustainable management of terrestrial ecosystems and rational use of natural resources (Zhang et al., 2022b). The Integrated Valuation of Ecosystem Services and Tradeoffs (InVEST) model provides a useful tool in monitoring and assessing ECS, given its low data requirements, fast computation speed, and high accuracy (Posner et al., 2016; Wei et al., 2021).

Land use patterns are the most pervasive and intuitive depiction of Earth's surface systems (Zhao et al., 2021). Land use scenario simulation, the cornerstone of research on ECS dynamics, is vital for ecosystem service evaluation (Wang et al., 2022c). Exploring future land use change and its impacts on ECS can assist decision-makers in developing rational ecological conservation plans. Simulation of land use change under multiple scenarios has implications for the optimization of low-carbon development. However, research on evaluating the impacts of land use change on ECS mostly and directly used the national carbon density data, which resulted in low estimation accuracy (Wang et al., 2022a); further, research that predicts future ECS under multiple land use scenarios is still insufficient (Chang et al., 2022; Lu et al., 2022).

In recent years, several generations of prediction models have been employed in land use scenario simulations (Leta et al., 2021; Liu et al., 2022). Many researchers have applied different land use simulation models to predict land use change (Zhao et al., 2019; Wang et al., 2022d; Li et al., 2023). These models are exemplified by the slope, land use, exclusion, urban extent, transportation, and hillshade (SLEUTH) model (Chaudhuri and Clarke, 2013), the conversion of land use and its effects at small regional extent (CLUE-S) model (Verburg et al., 2002), and the future land use simulation (FLUS) model (Liu et al., 2017). The cellular automata (CA) models can be used to simulate complex land use change (Xu et al., 2016), but most CA models focus too much on the improvement of simulation techniques and the correction of transformation rules (Cao et al., 2015). Consequently, these models play a limited role in exploring the causes of land use change (Sohl and Claggett, 2013) and lack the ability to simulate patch-level land use and landscape evolution (Meentemeyer et al., 2013). The patch-generating land use simulation (PLUS) model integrates a rule mining framework based on land expansion analysis and a CA model according to multi-type random seed mechanisms (Wang et al., 2022). This model allows researchers to identify the factors driving land expansion, predict the dynamic evolution of landscapes, and find the potential rules of land use change (Liang et al., 2021a). Compared with existing CA models, the PLUS model can simulate more similar landscape patterns with higher accuracy (Liang et al., 2021a), which can meet the requirements of future research on land use scenario simulation.

Approximately one third of the Earth's land area comprises arid and semi-arid areas (Raich and Schlesinger, 1992). As a major part of terrestrial ecosystems, arid and semi-arid areas play an integral role in the global carbon cycle (Lal, 2004). Owing to their fragile ecological environments, the land area of arid and semi-arid areas is likely to expand in the wake of global climate change (Maestre and Cortina, 2004). Land use change in arid and semi-arid areas inevitably imposes a profound influence on the global carbon balance (Hastings et al., 2005). The Ningxia Section of Yellow River Basin (NYRB) is a typical region dividing the arid and semi-arid climate zones in China (Li et al., 2021). It is an ecological barrier and corridor between the Chinese Loess Plateau and North China Plain. In the context of global warming and population growth, intensified land development and utilization activities in the NYRB have resulted in dramatic changes in land use and vegetation cover (Li et al., 2016). All natural and human factors may interact to influence the carbon cycle and balance, posing great challenges to the ecological environment of the NYRB. Given its unique geographical location and high ecological sensitivity, timely and accurate assessment of the impacts of land use change on ECS in the NYRB is crucial for regional ecological construction and high-quality development. It has been found that human activities were the key factors directly driving the spatiotemporal dynamics of land use in the

NYRB during 1985–2010 (Li et al., 2016). Although several studies have analyzed the land use change and associated dynamics of ECS in the NYRB (Li et al., 2021; Liang et al., 2021b; Zhu et al., 2022), no simulation of future land use change has been conducted in this region under multiple scenarios.

By coupling the InVEST and PLUS models, it is possible to simultaneously characterize the past evolution of regional ECS and predict its future trend under multiple land use scenarios. In this study, we calculated ECS using the InVEST model, and predicted land use patterns in the NYRB under multiple future scenarios using the PLUS model with historical data. We further evaluated the impacts of land use change on ECS during 1985–2020 and in 2050. The two models (InVEST and PLUS) were integrated to answer the following three questions: (1) How did the ECS change in the NYRB from 1985 to 2020? (2) How did land use change impact regional ECS during 1985–2020? (3) Which scenario (natural development or ecological protection) is favorable for improving future ECS in the river basin? This study is expected to provide useful information for achieving regional dual-carbon targets and formulating dual-carbon policies in arid and semi-arid areas. The results could provide guidance on ecological protection in arid and semi-arid areas.

2 Study area and data sources

2.1 Study area

The NYRB (35°49′25″–39°23′08″N, 104°17′04″–107°16′30″E; 956–3537 m; Fig. 1) consists of the main stream of Yellow River and its tributaries (e.g., Qingshui and Kushui rivers), accounting for nearly 80% of the total area of Ningxia Hui Autonomous Region, China. Its topography is complex and diverse, with the loess hilly area, mountain-plain area, and Ningxia Plain distributed from south to north, forming a three-stage topographic terrace. The remaining area of the NYRB is interspersed with deserts, plains, hills, and mountains. There are several nature reserves in the NYRB, such as the Helan Mountain National Nature Reserve, Baijitan National Nature Reserve, Luoshan National Nature Reserve, and Shapotou Nature Reserve. The mean annual temperature

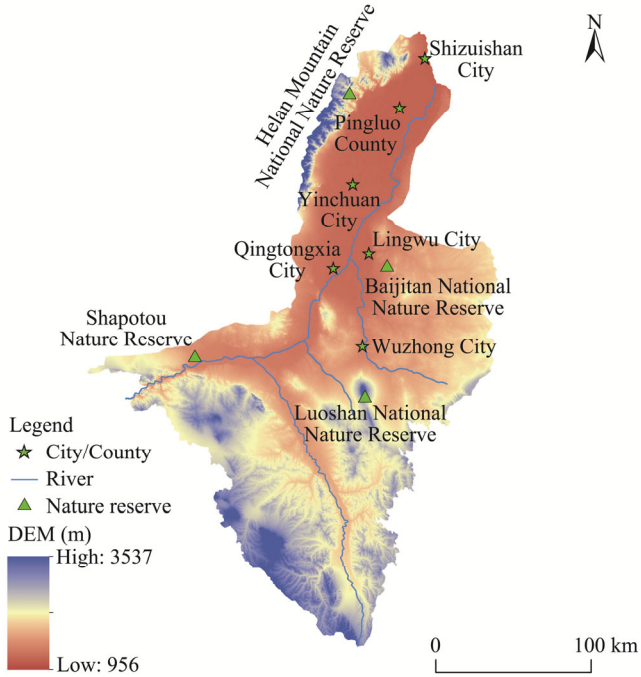

Fig. 1 Overview of the Ningxia Section of Yellow River Basin (NYRB) based on the digital elevation model (DEM)

here is between 11.5°C and 14.0°C. The mean annual precipitation is 200–800 mm with a non-uniform distribution, which is typical of a continental climate. The major land use types include cultivated land, woodland, grassland, water body, unused land, and construction land according to the utilization attributes of land resources. Among them, grassland can be subdivided into meadow grassland, typical grassland, and desert grassland according to the water and heat conditions. The soil types are mainly classified as Calcisol, Cambisol, Arenosol, Anthrosol, Fluvisol, Chernozem, Regosol, and Solonchak according to soil properties defined in terms of diagnostic horizons and characteristics.

2.2 Data sources

The historical data of land use and factors driving land use change in the study area were acquired from multiple sources (Table 1). Land use data (1985, 1990, 1995, 2000, 2005, 2010, 2015, and 2020) were reclassified into six primary categories, namely, cultivated land, woodland, grassland, water body, unused land, and construction land. Based on the study background and previous research (Liang et al., 2021b; Li et al., 2023), we selected 13 natural and human factors (Table 1), which were all used in the PLUS model. These data were uniformly preprocessed by projection transformation, clipping, and resampling in ArcGIS 10.2. Further preprocessing of transportation accessibility factors was performed using the Euclidean distance analysis tool in ArcGIS 10.2. To ensure data consistency, we uniformly resampled all data to the spatial resolution of 1 km×1 km, and adopted WGS_1984_UTM_Zone_48N as the projected coordinate system.

Table 1 Detailed description of data used in the study

Category/Indicator		Unit	Resolution	Time period	Source
Land use		-	30 m	1985–2020	https://zenodo.org/
Carbon density		t/hm^2	/	2010s	http://www.cern.ac.cn/
Natural factors	DEM	m	30 m	2009	https://earthexplorer.usgs.gov/
	Slope	°	30 m	2009	
	Aspect	-	30 m	2009	
	Annual mean temperature	°C	1 km	1990–2020	http://data.cma.cn/
	Annual precipitation	mm	1 km	1990–2020	
	Soil type	-	1 km	2010	http://www.resdc.cn/
	Vegetation type	-	1 km	2000	
Socioeconomic factors	Gross regional product	1×10^4 CNY/km^2	1 km	1985–2020	http://www.resdc.cn/
	Population distribution	persons/km^2	1 km	1985–2020	http://www.resdc.cn/
	Nighttime light	-	1 km	1990–2020	https://eogdata.mines.edu/products/dmsp
Transportation accessibility factor	Distance from roads, waterways, and residences	km	/	2020	https://www.openstreetmap.org/

Note: DEM, digital elevation model. "-" means no unit and "/" means no resolution.

3 Methods

3.1 Assessment of ECS

The carbon module of the InVEST v3.11.0 assesses ECS using land use as the unit of measurement for the land surface. We applied this module to assess the variations of ECS in the NYRB. We estimated the total ECS of the study area by multiplying the area of each land use type with its corresponding average carbon density based on Equation 1 (Piyathilake et al., 2022):

$$C_{\text{total}} = \sum_{i=1}^{n} A_i \left(C_{i\_\text{above}} + C_{i\_\text{below}} + C_{i\_\text{soil}} + C_{i\_\text{dead}} \right), \quad (1)$$

where C_{total} is the total ecosystem carbon storage (t); n is the number of land use types (n=6); A_i is the area of land use type i (hm^2); and C_{i_above}, C_{i_below}, C_{i_soil}, and C_{i_dead} are the aboveground, belowground, soil, and deadwood carbon densities (t/hm^2), respectively.

The InVEST model requires to input the carbon density data of different land use types. In this study, carbon density data were obtained from the dataset of carbon density in Chinese terrestrial ecosystems (2010s) at the National Ecosystem Science Data Center (http://www.cern.ac.cn) (Xu et al., 2019) and previous studies (Li et al., 2004; Xie et al., 2004; Huang et al., 2006; Chuai et al., 2011; Tang et al., 2018). We corrected these data to fit the actual data in the NYRB based on climatic conditions (Table 2) (Chen et al., 2007; Alam et al., 2013), and the correction equations are given by Equations 2–4:

$$C_{SP} = 3.3968 \times \mathrm{MAP} + 3996.1 \ (R^2 = 0.11), \tag{2}$$

$$C_{BP} = 6.798 \times \mathrm{e}^{0.0054 \times \mathrm{MAP}} \ (R^2 = 0.70), \tag{3}$$

$$C_{BT} = 28 \times \mathrm{MAT} \times 398 \ (R^2 = 0.47; P < 0.01), \tag{4}$$

where C_{SP} is the soil carbon density (Mg/hm^2); MAP is the mean annual precipitation (mm); C_{BP} and C_{BT} are the biomass carbon densities (Mg/hm^2) based on mean annual precipitation and mean annual temperature, respectively; MAT is the mean annual temperature (°C); and R^2 is the square of the correlation coefficient. The final carbon intensity correction equations are expressed by Equations 5–8 (Zhu et al., 2019; Bian et al., 2023):

$$K_{BP} = \frac{C'_{BP}}{C''_{BP}}, \tag{5}$$

$$K_{BT} = \frac{C'_{BT}}{C''_{BT}}, \tag{6}$$

$$K_B = K_{BP} \times K_{BT} = \frac{C'_{BP}}{C''_{BP}} \times \frac{C'_{BT}}{C''_{BT}}, \tag{7}$$

$$K_S = \frac{C'_{SP}}{C''_{SP}}, \tag{8}$$

where K_{BP} and K_{BT} are the correction coefficients for the biomass carbon density with mean annual precipitation and mean annual temperature, respectively; C'_{BP} and C''_{BP} are the biomass carbon densities (Mg/hm^2) obtained from the mean annual precipitation of the NYRB and Qihe River Basin (Zhang et al., 2022a); C'_{BT} and C''_{BT} are the biomass carbon densities (Mg/hm^2) based on the mean annual temperature of the NYRB and Qihe River Basin, respectively; K_B is the correction coefficient for biomass carbon density; K_S is the correction coefficient for soil carbon density; and C'_{SP} and C''_{SP} are the soil carbon densities (Mg/hm^2) obtained from the mean annual precipitation of the NYRB and Qihe River Basin, respectively. The reference data on carbon density were collected to obtain the carbon density data for different land use types (Table 2).

Table 2 Carbon density data of different land use types in the NYRB

Land use type	Carbon density (t/hm^2)			
	C_{i_above}	C_{i_below}	C_{i_soil}	C_{i_dead}
Cultivated land	3.72	8.33	92.39	0.00
Woodland	7.80	2.34	126.59	0.00
Grassland	1.37	5.07	96.66	0.00
Water body	0.00	0.00	0.00	0.00
Unused land	0.07	0.00	3.14	0.00
Construction land	0.02	0.00	0.00	0.00

Note: NYRB, Ningxia Section of Yellow River Basin. C_{i_above}, C_{i_below}, C_{i_soil}, and C_{i_dead} are the aboveground, belowground, soil, and deadwood carbon densities, respectively.

3.2 Future land use simulation

The PLUS model (HPSCIL@CUG, Wuhan, China) is a rule mining framework based on the land expansion analysis strategy coupled with a CA model using multiple random seeds (Wang et al., 2022d). This model can adapt to multiple types of land use patch adjustments in a flexible way, achieving greater simulation accuracy and landscape similarity than other models. In this study, we used the PLUS v1.3.5 to simulate future land use change under four different scenarios. More details (e.g., neighborhood weight parameter (Table S1) and land use transfer cost matrix (Table S2)) are available in the supplementary materials.

The detailed description on future land use scenario settings are as follows. First, the natural development scenario (NDS) represents a continuance of the historical trend of land use change. We used the Markov chain (Wang et al., 2022d) to simulate the area of each land use type in 2050 based on the land use transfer probability matrix (1990–2020) in the NYRB. The neighborhood weight parameter and transfer cost matrix of land use types in 2050 remained unchanged and were consistent with those during 1990–2020. Second, the ecological protection scenario (EPS) is based on the Land Spatial Planning of Ningxia Hui Autonomous Region (2021–2035) that aims to strengthen the protection of ecological land (e.g., woodland, grassland, and water body). Under this scenario, the probability of converting ecological land into construction land is reduced by 50%, and the probability of converting other land use types into ecological land is increased by 30%, with limited expansion of unused land and construction land. The areas of various land use types in 2050 under this scenario were predicted following the same method as those under the NDS, except that different neighborhood weight parameters were used. Third, the urban development scenario (UDS) focuses on urban development and construction, which promotes the conversion to construction land and restricts the conversion of construction land into other land use types. Therefore, the conversion probability of cultivated land, woodland, grassland, and unused land into construction land is increased by 20%, and the conversion probability of construction land into woodland, grassland, water body, and unused land is reduced by 30% to predict the land use scenario in the NYRB in 2050. Fourth, the cultivated land protection scenario (CPS) reduces the conversion probability of cultivated land into other land use types by 50%, with other land use types still maintaining their natural development trend.

3.3 Driving factor analysis

The geographical detector (Geodetector) is a statistical tool to explore the spatial differentiation in geographical phenomena and detect the driving factors (Wang and Xu, 2017). Land use type is a model factor closely related to ECS. Therefore, we excluded the model factor (land use type) and selected the nighttime light (which represents the intensity of human activities at global and regional scales) and natural factors (i.e., annual precipitation, annual mean temperature, digital elevation model (DEM), slope, aspect, vegetation type, and soil type) as the independent variables. The factor detector and the interaction detector in the Geodetector were used to quantitatively analyze the influences of various factors and identify their interactions on ECS.

3.3.1 Factor detection

The influence of each selected driving factor (independent variable X) on ECS (dependent variable Y) was evaluated using the q-statistic (Eq. 9):

$$q = 1 - \frac{\sum_{h=1}^{L} N_h \sigma_h^2}{N\sigma^2} = 1 - \frac{SSW}{SST}, \tag{9}$$

where q-statistic indicates the influence of independent variable X on dependent variable Y (q=[0, 1]; the stronger the explanatory power of independent variable X to dependent variable Y, the higher the q-statistic, and vice versa); h is the classification or partition of dependent variable Y or independent variable X; L is the number of layers of the variable; N_h and N are the unit numbers

of class h and the entire region, respectively; σ_h^2 and σ^2 are the variances of dependent variable Y in class h and the whole area, respectively; and SSW and SST are the within sum of squares and the total sum of squares, respectively.

3.3.2 Interaction detection

The interaction between various factors on ECS was identified to determine whether the combination of factors X_1 and X_2 could enhance or attenuate their explanatory power for ECS (dependent variable Y), or whether the influence of these factors on dependent variable Y is independent of each other. Table 3 shows the five types of factor interactions (Wang and Xu, 2017) considered in this study.

Table 3 Interaction types of the factors driving the spatial differentiation of ecosystem carbon storage (ECS)

Interaction type	Judgment criteria
Nonlinear attenuation	$q(X_1 \cap X_2) < \min[q(X_1), q(X_2)]$
Univariate nonlinear attenuation	$\min[q(X_1), q(X_2)] < q(X_1 \cap X_2) < \max[q(X_1), q(X_2)]$
Bivariate enhancement	$q(X_1 \cap X_2) > \max[q(X_1), q(X_2)]$
Nonlinear enhancement	$q(X_1 \cap X_2) > q(X_1) + q(X_2)$
Independent	$q(X_1 \cap X_2) = q(X_1) + q(X_2)$

Note: X_1 and X_2 are the influencing factors; $q(X_1)$ and $q(X_2)$ represent the influences of factors X_1 and X_2 on the spatial differentiation of ECS, respectively; $q(X_1 \cap X_2)$ represents the influence of the interaction between factors X_1 and X_2 on the spatial differentiation of ECS.

4 Results

4.1 Temporal and spatial variation characteristics of ECS

During 1985–2020, the total ECS in the study area increased from 1985 until reaching a peak at 402.36×10^6 t in 2010 and then slightly decreased from 2010 to 2020 (Table 4). The ECS increased by 16.99×10^6 t (4.41%) from 1985 to 2010 with an average growth rate of 0.68×10^6 t/a (0.18%/a), and the highest growth rate was 1.74×10^6 t/a (0.45%/a) during 1990–1995. The ECS decreased by 3.87×10^6 t (0.96%) from 2010 to 2020, with an average reduction rate of 0.39×10^6 t/a (0.10%/a).

Table 4 Total ECS in the NYRB during 1985–2020

Year	1985	1990	1995	2000	2005	2010	2015	2020
ECS ($\times 10^6$ t)	385.37	385.81	394.48	396.86	401.81	402.36	399.53	398.49

Spatial variation analysis revealed that ECS basically decreased from south to north and from east to west in the study area (Fig. 2). Areas with high ECS were distributed in the southern loess hills and valleys, the central arid zone, and the northern Helan Mountain National Nature Reserve, which mainly comprised woodland, grassland, and cultivated land with high carbon sequestration capacity. However, areas with low ECS were distributed in the economic zone along the Yellow River, which were dominated by construction land and water body with low carbon sequestration capacity.

Three different variation types (increased, unchanged, and decreased) were analyzed to explore the spatial distribution of the variations in ECS during 1985–2020 (Fig. 3). The ECS showed markedly spatial variations during 1985–2010 and 2010–2020. In the first period (1985–2010), increased ECS was observed in 7.10% of the study area, mainly in the Shapotou Nature Reserve, southern Helan Mountain National Nature Reserve, Qingtongxia City, and Baijitan National Nature Reserve; decreased ECS was observed in 2.93% of the study area, which appeared in a scattered distribution in the urban areas of Yinchuan City, Wuzhong City, and Shizuishan City, in addition to other counties and districts with fast economic development. In the second period (2010–2020), only 1.92% of the study area showed increased ECS, mainly in the eastern Baijitan National Nature Reserve and Pingluo County. Additionally, 2.71% of the study area (1214.02 km^2) showed decreased ECS, which was concentrated in Qingtongxia City.

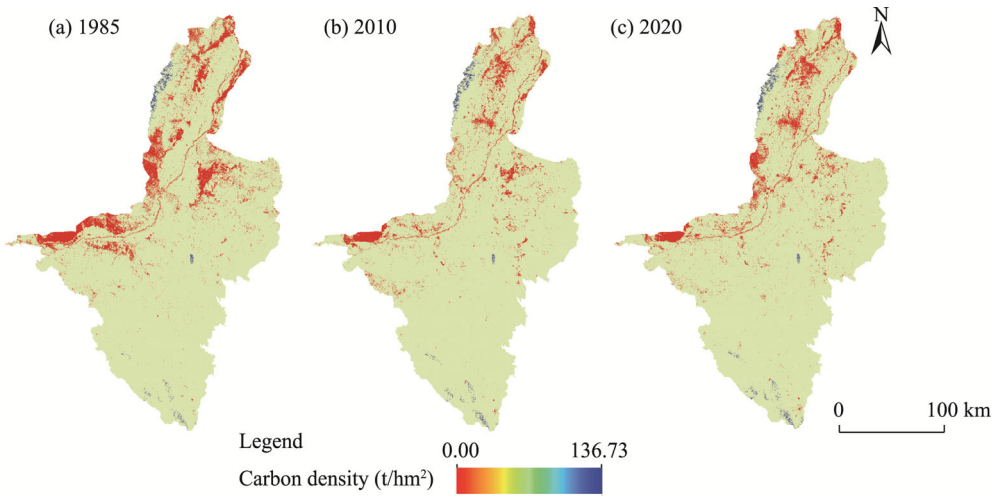

Fig. 2 Spatial distribution of ECS (indicated by carbon density) in the NYRB in 1985 (a), 2010 (b), and 2020 (c)

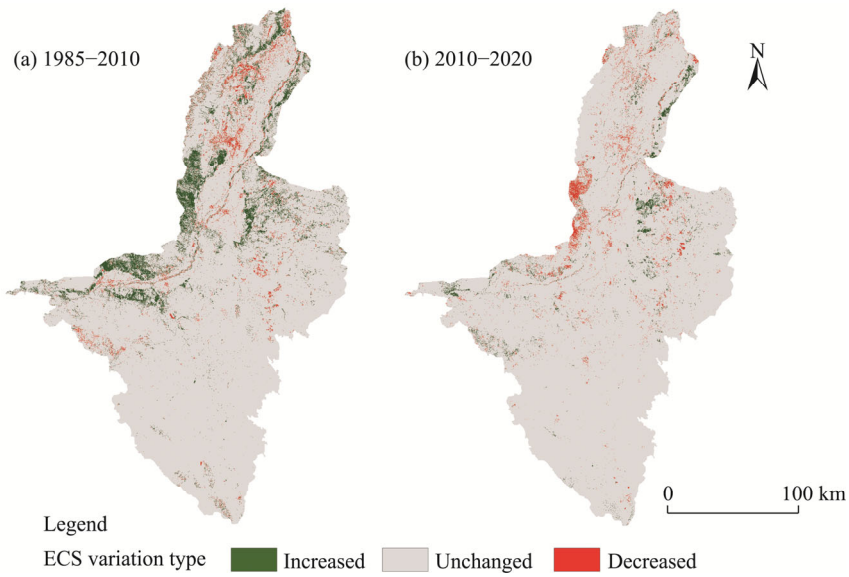

Fig. 3 Spatial distribution of the variations in ECS in the NYRB during 1985–2010 (a) and 2010–2020 (b)

4.2 Impacts of land use change on ECS

Table 5 shows the ECS in the NYRB under different land use types, and it can be found that grassland was the most important carbon pool during 1985–2020, with ECS accounting for >70.00% of the total ECS in the study area. Cultivated land showed the second highest carbon sequestration capacity, and its ECS was equivalent to only one-third of the ECS of grassland. The ECS of woodland and unused land ranked in descending order, and the ECS of construction land and water body was almost zero. From 1985 to 2020, the area of construction land continued to increase, but its total ECS remained zero. This was mainly due to the accelerated urbanization in the NYRB and the continued expansion of construction land with low carbon sequestration capacity. From 1985 to 2010, grassland, cultivated land, and woodland all expanded, which respectively contributed 82.75%, 19.54%, and 2.12% to the increase in the total ECS in the study area. This was the primary reason for the upward trend of the total ECS in the NYRB during 1985–2010. From 2010 to 2020, the total ECS showed a downward trend, which was mainly resulted from grassland reduction and construction land expansion.

Table 5 ECS of different land use types in the NYRB during 1985–2020

Land use type	ECS ($\times 10^6$ t)							
	1985	1990	1995	2000	2005	2010	2015	2020
Cultivated land	96.35	97.15	109.80	108.87	92.24	99.67	97.47	104.84
Woodland	2.46	2.49	2.70	2.77	2.80	2.82	2.91	3.13
Grassland	285.30	284.93	281.02	284.36	306.15	299.36	298.61	289.98
Unused land	1.26	1.24	0.96	0.86	0.62	0.51	0.54	0.54
Construction land	0.00	0.00	0.00	0.00	0.00	0.00	0.00	0.00

Figure 4 shows the land use type transfer in the NYRB during 1985–2010 and 2010–2020. Overall, land use change in the NYRB was dominated by the expansion of cultivated land, woodland, and construction land at the expense of unused land. In the first period (1985–2010), an area of 2613.98 km^2 land was transferred into cultivated land, with the majority from grassland (85.26% of the transfer-in area of cultivated land) and small proportions from unused land (10.84%), water body (3.76%), and construction land (0.14%). A similar trend was observed in the second period (2010–2020), with an area of 2093.62 km^2 land transferred into cultivated land, mainly from grassland (93.23%). The transfer-in area of woodland was 28.25 km^2 in the first period and 22.21 km^2 in the second period, predominantly transferred from grassland (96.05% and 93.55% of the transfer-in area of woodland, respectively). The transfer-in area of construction land reached 563.64 km^2 in the first period, mainly from cultivated land (50.88% of the transfer-in area of construction land), grassland (27.34%), and unused land (20.25%). In the second period, an area of 296.61 km^2 land was transferred into construction land, with 50.51% from cultivated land, 24.38% from grassland, and 3.21% from unused land.

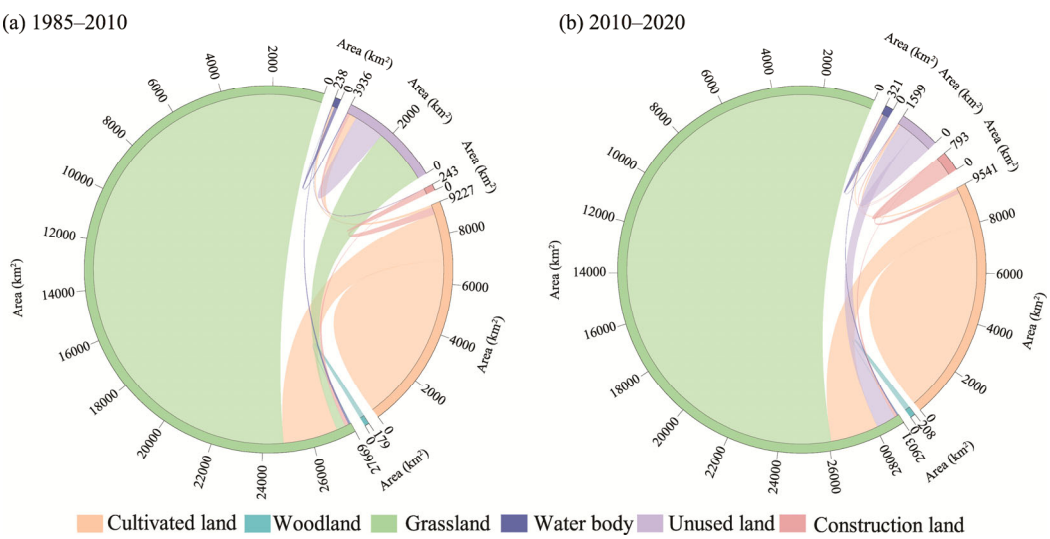

Fig. 4 Chord diagrams of mutual conversion of different land use types in the NYRB during 1985–2010 (a) and 2010–2020 (b)

The transfer-out area of unused land was 2709.61 km^2 during 1985–2010 and 739.55 km^2 during 2010–2020; unused land in the two periods was largely transferred into grassland (84.37% and 84.25% of the transfer-out area of unused land, respectively), with small proportions transferred into cultivated land (10.46% and 10.21%, respectively) and construction land (4.21% and 4.69%, respectively) (Fig. 4). Furthermore, the area of grassland initially expanded and then reduced, with a slight increasing trend over the 36-year study period. From 1985 to 2010, the transfer-in area of grassland was 4203.10 km^2, of which 54.39% was transferred from unused land

and 45.38% from cultivated land. Conversely, from 2010 to 2020, 2926.63 km^2 of grassland area was transferred out, of which 66.70% was transferred into cultivated land, 27.73% into unused land, and 3.48% into construction land. Water body expanded over time; specifically, the transferred-in area was 202.50 km^2 in the first period and 115.74 km^2 in the second period. Water body in the two periods was mainly transferred from cultivated land (46.09% and 52.44% of the transfer-in area of water body, respectively) and grassland (34.89% and 34.77%, respectively). Overall, land use change between 1985 and 2020 was dominated by the transfer of unused land with lower carbon density to grassland with higher carbon density, and the latter land use type was synchronously converted into cultivated land with higher carbon density.

4.3 Temporal and spatial variation characteristics of land use change and ECS under land use scenarios

4.3.1 Accuracy of land use simulation

To evaluate the simulation results of land use distribution in 2050, we used the land use data of 1990 as the training set for simulating the land use distribution in 2020 (Fig. 5). The Kappa coefficient was 0.832 and the overall accuracy was 0.910, suggesting that the simulation results were highly consistent with the actual land use distribution. Therefore, the land use simulation model was feasible and credible to meet the research needs.

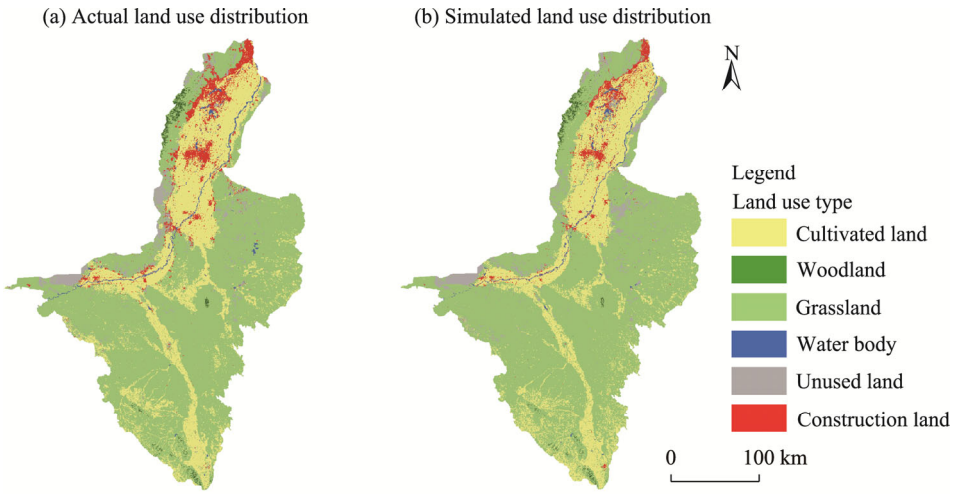

Fig. 5 Spatial distribution of actual (a) and simulated (b) land use distribution in the NYRB in 2020

4.3.2 Future patterns of land use change under land use scenarios

Changes in land use types were predicted to have similar patterns during 2020–2050 under the four different land use scenarios (Table 6). Compared to 2020, the area of grassland will decrease by 6.22% in 2050 under the NDS, whereas the areas of cultivated land, woodland, and construction land will increase by 8.50%, 24.98%, and 74.29%, respectively. Under the EPS, the shrinkage of grassland in 2050 will diminish compared to that under the NDS; the area of grassland will decrease by 4.38% in 2050 compared to 2020, while the areas of woodland and water body will increase by 42.68% and 28.06%, respectively. Construction land will expand remarkably under the UDS, with its area increasing from 1081.30 km^2 in 2020 to 2889.45 km^2 in 2050. The area of cultivated land will reach its maximum extent under the CPS (increasing by 19.80% in 2050 compared to 2020), whereas the area of grassland will decrease by 9.92% in 2050 compared to 2020.

4.3.3 Temporal and spatial variation characteristics of ECS under land use scenarios

Table 7 summarizes the prediction results of ECS in 2050 under the four land use scenarios based on the InVEST model. Among them, the lowest ECS will occur under the UDS (378.85×10^6 t), while the highest is under the EPS (396.26×10^6 t). The ECS under the NDS and CPS will reach

Table 6 Area of land use change in the NYRB during 2020–2050 under the four land use scenarios

Land use type	Area of land use change (km^2)							
	NDS		EPS		UDS		CPS	
	2050	2020–2050	2050	2020–2050	2050	2020–2050	2050	2020–2050
Cultivated land	10,800.85	766.14	10,800.85	766.14	10,802.85	766.14	11,927.94	1891.23
Woodland	282.43	54.01	322.42	94.00	282.43	54.01	302.43	74.01
Grassland	26,491.05	–1634.30	27,009.03	–1112.32	25,459.26	–2662.09	25,443.97	–2677.38
Water body	404.89	60.27	444.89	100.27	404.89	60.27	404.89	60.27
Unused land	1654.11	–26.48	1554.12	–126.47	1654.11	–26.48	1554.12	–126.47
Construction land	1859.66	778.36	1359.69	278.38	2889.45	1808.15	1859.64	778.34

Note: NDS, natural development scenario; EPS, ecological protection scenario; CPS, cultivated land protection scenario; UDS, urban development scenario.

Table 7 ECS of different land use types in the NYRB in 2050 under the four land use scenarios

Land use type	ECS ($\times 10^6$ t)			
	NDS	EPS	UDS	CPS
Cultivated land	112.84	112.84	112.84	124.60
Woodland	3.86	4.41	2.95	3.16
Grassland	273.15	278.51	262.53	262.37
Unused land	0.53	0.50	0.53	0.50
Construction land	0.00	0.00	0.00	0.00
Total carbon storage	390.38	396.26	378.85	390.63

similar levels, at 390.38×10^6 and 390.63×10^6 t, respectively. The total ECS in 2050 under all scenarios will be lower than that in 2020 (Tables 5 and 7).

Under all scenarios, the spatial distribution of ECS in 2050 will show high values in the southern part of the study area and low values in the northern part (Fig. 6a–d). The variations in ECS during 2020–2050 will predominantly occur in the economic zone along the Yellow River (Fig. 6e–h). Specifically, there will be a decrease in ECS in 2.64% of the study area (1095.41 km^2) under the NDS, mainly in cities with fast economic development, such as Yinchuan City and Wuzhong City. Additionally, 0.72% of the study area (297.02 km^2) will show an increase in ECS under the NDS, primarily in the western part of Qingtongxia City and Lingwu City.

Compared with ECS under the NDS, there will be larger areas showing a decrease (1526.09 km^2, i.e., 3.68% of the total area) or an increase (1327.63 km^2, i.e., 3.20% of the total area) in ECS under the EPS. This indicates that the adoption of ecological protection strategies will lead to a remarkable expansion of areas with increased ECS while diminishing the decrease in the total ECS in the NYRB. The ECS will decrease in considerable areas (4948.46 km^2, i.e., 11.93% of the total area) under the UDS, accelerating the decline of the total ECS in the study area. The variation trend of ECS under the CPS is consistent with that under the NDS. The ECS will decrease in 9.20% of the study area (3818.65 km^2) under the CPS, whereas an area of 302.43 km^2 (0.73% of the study area) will exert an increase in ECS.

4.4 Influence factors driving the spatial differentiation of ECS

4.4.1 Influence of individual natural and human factors

The natural and human factors had distinct influences on the spatial differentiation of ECS in the NYRB (Fig. 7). We ranked the influences of various factors based on the *q*-statistic values: nighttime light>soil type>annual mean temperature>annual precipitation>DEM>slope>vegetation type>aspect. Nighttime light was the leading factor contributing to the spatial differentiation of ECS (q=0.322). Soil type and annual mean temperature (q>0.200 for each) were the major natural factors driving the spatial differentiation of ECS. Annual precipitation and DEM (q>0.100 for each), followed by slope, vegetation type, and aspect (q<0.100 for each), were less influential in shaping the spatial distribution of ECS.

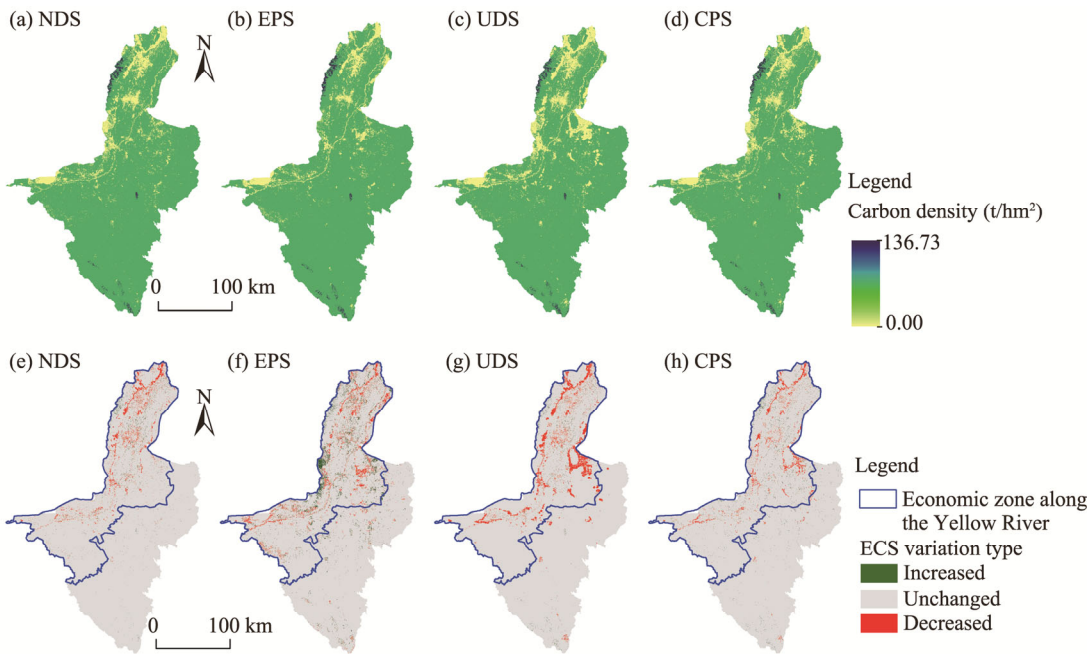

Fig. 6 Spatial distribution patterns of ECS (indicated by carbon density; a–d) in 2050 and variations in ECS during 2020–2050 (e–h) in the NYRB. (a), ECS under the NDS in 2050; (b), ECS under the EPS in 2050; (c), ECS under the UDS in 2050; (d), ECS under the CPS in 2050; (e), variations in ECS under the NDS during 2020–2050; (f), variations in ECS under the EPS during 2020–2050; (g), variations in ECS under the UDS during 2020–2050; (h), variations in ECS under the CPS during 2020–2050. NDS, natural development scenario; EPS, ecological protection scenario; UDS, urban development scenario; CPS, cultivated land protection scenario.

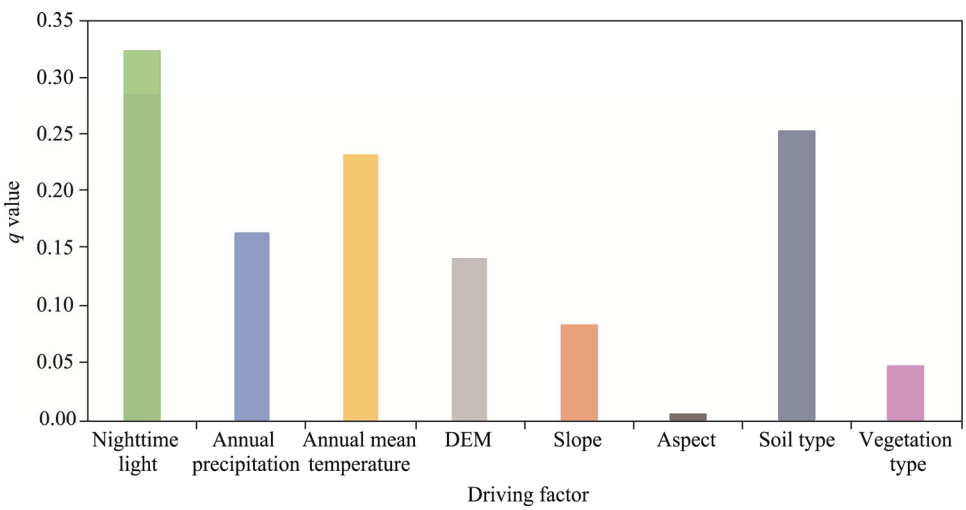

Fig. 7 Results of factor detector in the geographical detector (Geodetector) analysis showing the influence of each driving factor on the spatial differentiation of ECS in 2020. The *q* value indicates the influence of each driving factor on the spatial differentiation of ECS.

4.4.2 Interactions between influence factors and their combined effect on the spatial differentiation of ECS

Overall, the interactions between natural and human factors exhibited an enhancement effect on the spatial differentiation of ECS (Fig. 8). The interactions of two driving factors that affected the spatial distribution of ECS showing nonlinear enhancement accounted for 87.50%, and bivariate enhancement accounted for 12.50%. There were no independent factors, indicating that the

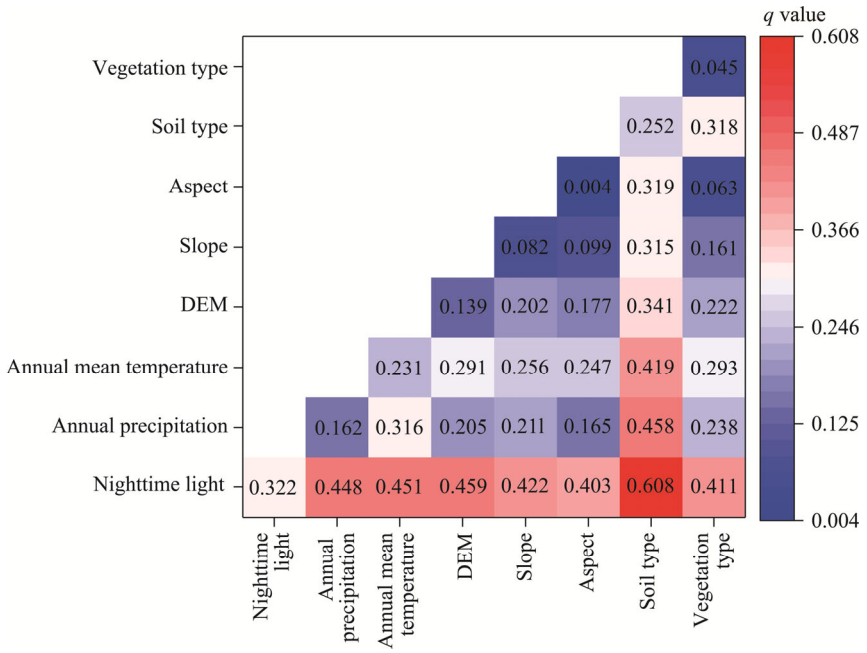

Fig. 8 Results of interaction detector in the Geodetector analysis showing the combined effect of any two driving factors on the spatial differentiation of ECS in 2020

influence of the interaction between any two driving factors on the spatial differentiation of ECS was greater than that of a single driving factor in the NYRB. Among the eight different driving factors, the interaction between nighttime light and soil type had the greatest influence on the spatial differentiation of ECS (q=0.608), followed by the interaction between DEM and nighttime light (q=0.459) and the interaction between soil type and annual precipitation (q=0.458) (Fig. 8). Despite the low explanatory power of natural factors such as slope and aspect, their interaction with nighttime light showed a strong influence on the spatial differentiation of ECS (q values of 0.422 and 0.403, respectively). The combined effect between other natural factors and nighttime light was also non-negligible (q>0.400), providing additional evidence for the strong influence of human activities on the spatial differentiation of ECS. The results indicate that the influence of various natural and human factors was nonlinearly and interactively enhanced through interactions, and the complex coupling between various influence factors shaped the spatial differentiation of ECS.

5 Discussion

5.1 Temporal and spatial variation characteristics of ECS caused by land use change

Ecosystems in arid and semi-arid areas constitute a significant portion of the global carbon pool and therefore considerably contribute to the carbon biogeochemical cycling (Gu et al., 2018). The carbon dynamics in arid and semi-arid areas can mitigate or enhance the environmental impacts of atmospheric CO_2 and global drought (Dai et al., 2019). It is vital to reveal the temporal and spatial variation characteristics of ECS in representative arid and semi-arid areas, such as the NYRB. Yang et al. (2021) found that the total carbon storage in the Yellow River Basin exhibited an upward trend from 2000 to 2018, which mirrors the patterns observed in the NYRB (this study) and in the upper reaches of Shule River Basin, China (Wei et al., 2021). Additionally, Wang et al. (2020) found that the soil carbon storage of desert grasslands in Ningxia Hui Autonomous Region accumulated at a rate of 2.00 g/(m^2·a), and the total ECS basically increased from 1958 to 2017. In partial support of the previous findings, we found that the total ECS in the NYRB increased by 13.71×10^6 t from 1985 to 2020, despite a downward trend during 2010–2020.

In the NYRB, the dominant grassland type is desert grassland, which features slightly lower carbon density than cultivated land (Fig. 4). In the wake of continuous population growth, the transformation of grassland and unused land to cultivated land has led to a considerable increase in ECS during 1985–2010 (Table 5). Since 2000, China has implemented the Strategy for Large-scale Development of Western China, and the government in Ningxia Hui Autonomous Region has accelerated the pace of converting cultivated land into woodland and grassland (Li et al., 2012). Consequently, the area of cultivated land in the NYRB decreased over time and was largely converted into grassland (Fig. 4; Table 5). Moreover, western China has been experiencing rapid industrialization and urbanization, with land use change being intensified over time (Li et al., 2012). During the study period, the population size and construction land area in the NYRB have been growing dramatically, especially in the economic zone along the Yellow River (Lyu et al., 2019). As a result, the ECS in the study area decreased from 2010 to 2020 (Table 4), indicating that the ecosystems in arid and semi-arid areas have changed from a carbon sink to a carbon source, with a functional decline in carbon sequestration.

With regard to land use change, Li et al. (2016) found that from 1985 to 2010, the area of woodland, construction land, and cultivated land expanded at the expense of unused land in the NYRB, which is compatible with our findings. Large-scale conversion of unused land with low carbon density into grassland and cultivated land with high carbon density was the primary factor leading to the increase in ECS over the period of 1985–2010. In recent decades, land use patterns have markedly changed in the NYRB owing to the implementation of ecological protection projects, such as the Returning Farmland to Forest or Grassland and Sand Control & Forest Protection (Wu et al., 2020), which is conducive to carbon sequestration. Overall, the land use structure of the NYRB has been optimized over the 36-year study period, with a considerable expansion of woodland and water body and a simultaneous shrinkage of unused land.

We found that ECS showed regional differences in its spatial distribution across the NYRB. The Shapotou Nature Reserve and Baijitan National Nature Reserve are located at the edge of Tengger Desert and Mu Us Sandy Land, respectively. Yang and Wang (2009) and Song et al. (2021) found that the two nature reserves were devoted to ecological restoration, evolving the original drifting sandy land into an artificial-natural composite desert-vegetation landscape through sand control and afforestation. We also found that the dominant land use type in the two nature reserves changed from unused land to grassland from 1985 to 2020, along with a steady increase in ECS (Fig. 3). Furthermore, the NYRB is an ecologically fragile inland region in northwestern China, and water shortage is the most important ecological limiting factor in this region. Barren mountains and slope areas at the edge of Qingtongxia City are located in the border zone between Ningxia Hui Autonomous Region and Inner Mongolia Autonomous Region, far from cities and suburbs. Their ecological environment is highly sensitive to external disturbances, and large areas of unused land have been transformed into grassland under ecological protection projects, contributing to the increased ECS from 1985 to 2010. However, after 2010, the ECS in these sensitive areas decreased to a certain degree, which is probably a result of grassland degradation under reduced precipitation.

5.2 Quantification analysis of factors driving the spatial differentiation of ECS

Previous studies have shown that land use change is the main factor affecting the variation in ECS (Lai et al., 2016; Nie et al., 2020; Wang et al., 2022d). In this study, we used land use as a model factor and excluded it from the analysis of influence factors driving the change in ECS. Nighttime light can indicate the intensity of human activities at global and regional scales, so we used this index as a human factor to represent socioeconomic condition and transportation accessibility. Our results provide an evidence that nighttime light strongly influences the ECS in the NYRB.

We found that soil type and annual mean temperature are the major natural factors driving the spatial differentiation of ECS, in agreement with previous studies (Wiesmeier et al., 2015; Xu et al., 2018). From a geographical perspective, soil nutrients directly affect soil carbon storage, and higher nutrient contents generally contribute to larger soil carbon storage (Dignac et al., 2017).

Soil nutrients also support plant growth and biomass accumulation, thereby improving vegetation carbon density and carbon storage. From a meteorological perspective, higher temperatures accelerate the carbon sequestration, since a chemical process takes place at a faster rate under higher-temperature conditions (Elbasiouny et al., 2022). Our results reveal that the interaction of any two driving factors had a greater influence on ECS compared to a single driving factor, indicating that the spatial variation in regional ECS has arisen from the combined effect of multiple influence factors (Huo and Sun, 2021; Xiang et al., 2022).

5.3 Suggestions for optimizing future land use patterns

Based on the PLUS model, we predicted the variation of ECS in the NYRB under four future land use scenarios. The ECS will exhibit a downward trend from 2020 to 2050 under both the NDS and EPS, which may be related to the lagging economic development of Ningxia Hui Autonomous Region and its large economic gap compared with other developed regions in China (Yang et al., 2018). Specifically, the future decrease in ECS can be attributable to the accelerated urbanization of the NYRB, the large-scale conversion of cultivated land and grassland with high carbon density into construction land with low carbon density, and the depletion of reclaimable unused land. Grassland is the most dominant land use type in the NYRB, accounting for more than 65.00% of the total study area (Fig. 5; Table 6). As animal husbandry is the pillar industry of the regional economy, grassland is frequently affected by human activities (Lu et al., 2017). Therefore, grassland conservation is the key to achieving sustainable ecosystem development and promoting carbon sequestration in the NYRB.

The ranking of the total ECS in the NYRB under the four land use scenarios (i.e., EPS>CPS>NDS>UPS) is consistent with the results of Bian et al. (2023). Considering the variation of ECS in the NYRB under different land use scenarios, decision-makers should focus on protecting grassland resources and preventing grassland degradation, in addition to limiting the expansion of construction land. Furthermore, approaches for the optimization of low-carbon-oriented land use structure should be adopted, and the transformation of unused land into woodland or grassland needs to be promoted by exploiting unused land, establishing no-grazing protection zones, and strengthening legal grassland and woodland management. It is also suggested to consolidate the achievements of ecological construction in grassland.

In the next 30 years, variation in ECS will occur mainly in the economic zone along the Yellow River, a nationally important ecological node and the core area for the construction of the early ecological protection zone in the NYRB. In areas with fast economic development, ECS will decrease due to rapid regional urbanization, industrialization, and population growth along both sides of Yellow River. In contrast, ECS will be effectively increased in areas where ecological conservation and restoration projects have been vigorously promoted, such as wetlands along the Yellow River, forests, and scrubland. Therefore, in addition to limiting construction land expansion and enhancing nature reserve conservation, decision-makers should strengthen the biological engineering programs in western Qingtongxia City and northern Shapotou Nature Reserve to control the erosion of wind and sand from the Tengger Desert. Furthermore, it is recommended to promote the conversion of unused land in to grassland using genetically improved grass seeds in Lingwu City and Pingluo County (Du, 2020).

6 Conclusions

This study characterized the current and future spatiotemporal variations of ECS in response to land use change in the NYRB by coupling the PLUS model and InVEST model. The total ECS in the study area increased from 385.37×10^6 t in 1985 to 398.49×10^6 t in 2020, with a growth rate of 3.40% and a peak value of 402.36×10^6 t (2010). The ECS showed a heterogeneous spatial distribution and decreased overall from south to north. The spatiotemporal patterns of ECS were prominently influenced by the inter-conversion between unused land with low carbon density and grassland (and cultivated land) with high carbon density. In addition to human activities, soil type

and annual mean temperature had a strong influence on the spatial differentiation of ECS. Compared with the situation in 2020, the total ECS in 2050 will further decrease under different future land use scenarios with the order of EPS>CPS>NDS>UDS.

ECS assessment results in the NYRB are beneficial to decision-making in regional ecological protection and sustainable development. The carbon density could vary depending on environmental change and human activities, which calls for field studies to continuously monitor the carbon density and verify the reliability of the corrected data in a timely manner. To improve the accuracy of land use simulations, the impact of policy factors (e.g., ecological protection red line) on land use change should be taken into account in future research, as such factors could affect the performance of the PLUS model. Findings of this study could provide theoretical support for future carbon management and territorial spatial planning in the study area as well as other similar arid and semi-arid areas.

Conflict of interest

The authors declare that they have no known competing financial interests or personal relationships that could have appeared to influence the work reported in this paper.

Acknowledgements

This study was supported by the Innovation Projects for Overseas Returnees of Ningxia Hui Autonomous Region-Study on Multi-Scenario Land Use Optimization and Carbon Storage in the Ningxia Section of Yellow River Basin (202303), the National Natural Science Foundation of China (42067022, 41761066), and the Natural Science Foundation of Ningxia Hui Autonomous Region, China (2022AAC03024).

Author contributions

Conceptualization: LIN Yanmin; Methodology: LIN Yanmin, HU Zhirui, LI Wenhui; Formal analysis: LIN Yanmin, HU Zhirui, LI Wenhui, CHEN Haonan; Writing - original draft preparation: LIN Yanmin, HU Zhirui; Writing - review and editing: LIN Yanmin; WANG Fang, NAN Xiongxiong; Funding acquisition: WANG Fang, NAN Xiongxiong; Resources: YANG Xuelong, ZHANG Wenjun; Supervision: WANG Fang, NAN Xiongxiong. All authors approved the manuscript.

References

Alam S A, Starr M, Clark B J F. 2013. Tree biomass and soil organic carbon densities across the Sudanese woodland savannah: A regional carbon sequestration study. Journal of Arid Environments, 89: 67–76.

Bian R, Zhao A T, Liu X F, et al. 2023. Impact of land use change on carbon storage in urban agglomerations in the Guanzhong plain. Environmental Science, doi: 10.13227/j.hjkx.202306233. (in Chinese)

Cao M, Tang G A, Shen Q F, et al. 2015. A new discovery of transition rules for cellular automata by using cuckoo search algorithm. International Journal of Geographical Information Science, 29(5): 806–824.

Chang X Q, Xing Y Q, Wang J Q, et al. 2022. Effects of land use and cover change (LUCC) on terrestrial carbon stocks in China between 2000 and 2018. Resources, Conservation and Recycling, 182: 106333, doi: 10.1016/j.resconrec.2022.106333.

Chaudhuri G, Clarke K. 2013. The SLEUTH land use change model: A review. Environmental Resources Research, 1(1): 88–105.

Chen G S, Yang Y S, Xie J S, et al. 2007. Total belowground carbon allocation in China's forests. Acta Ecologica Sinica, 27(12): 5148–5157. (in Chinese)

Chuai X W, Huang X J, Zheng Z Q, et al. 2011. Land use change and its influence on carbon storage of terrestrial ecosystems in Jiangsu Province. Resources Science, 33(10): 1932–1939. (in Chinese)

Dai L C, Ke X, Guo X W, et al. 2019. Responses of biomass allocation across two vegetation types to climate fluctuations in the northern Qinghai–Tibet Plateau. Ecology and Evolution, 9(10): 6105–6115.

Dignac M F, Derrien D, Barré P, et al. 2017. Increasing soil carbon storage: mechanisms, effects of agricultural practices and proxies. A review. Agronomy for Sustainable Development, 37(2): 14, doi: 10.1007/s13593-017-0421-2.

Dong F, Li J Y, Wang Y, et al. 2019. Drivers of the decoupling indicator between the economic growth and energy-related CO_2

in China: A revisit from the perspectives of decomposition and spatiotemporal heterogeneity. Science of the Total Environment, 685: 631–658.

Du X G. 2020. Improvement status and suggestions of degraded natural grassland in Sunan County. Journal of Animal Science and Veterinary Medicine, 39(4): 70–71. (in Chinese)

Elbasiouny H, El-Ramady H, Elbehiry F, et al. 2022. Plant nutrition under climate change and soil carbon sequestration. Sustainability, 14(2): 914, doi: 10.3390/su14020914.

Gu Q, Wei J, Luo S C, et al. 2018. Potential and environmental control of carbon sequestration in major ecosystems across arid and semi-arid regions in China. Science of the Total Environment, 645: 796–805.

Hastings S J, Oechel W C, Muhliamelo A. 2005. Diurnal, seasonal and annual variation in the net ecosystem CO_2 exchange of a desert shrub community (Sarcocaulescent) in Baja California, Mexico. Global Change Biology, 11(6): 927–939.

He C Y, Zhang D, Huang Q X, et al. 2016. Assessing the potential impacts of urban expansion on regional carbon storage by linking the LUSD-urban and InVEST models. Environmental Modelling & Software, 75: 44–58.

Houghton R A. 2003. Revised estimates of the annual net flux of carbon to the atmosphere from changes in land use and land management 1850–2000. Tellus B: Chemical and Physical Meteorology, 55(2): 378–390.

Huang M, Ji J J, Cao M K, et al. 2006. Modeling study of vegetation shoot and root biomass in China. Acta Ecologica Sinica, 26(12): 4156–4163. (in Chinese)

Huo H, Sun C P. 2021. Spatiotemporal variation and influencing factors of vegetation dynamics based on Geodetector: A case study of the northwestern Yunnan Plateau, China. Ecological Indicators, 130: 108005, doi: 10.1016/j.ecolind.2021.108005.

Lai L, Huang X J, Yang H, et al. 2016. Carbon emissions from land-use change and management in China between 1990 and 2010. Science Advances, 2(11): e1601063, doi: 10.1126/sciadv.1601063.

Lal R. 2004. Carbon sequestration in dryland ecosystems. Environmental Management, 33(4): 528–544.

Leta M K, Demissie T A, Tränckner J. 2021. Modeling and prediction of land use land cover change dynamics based on land change modeler (LCM) in Nashe watershed, Upper Blue Nile Basin, Ethiopia. Sustainability, 13(7): 3740, doi: 10.3390/su13073740.

Li K M, Cao J J, Adamowski J F, et al. 2021. Assessing the effects of ecological engineering on spatiotemporal dynamics of carbon storage from 2000 to 2016 in the Loess Plateau area using the InVEST model: A case study in Huining County, China. Environmental Development, 39: 100641, doi: 10.1016/j.envdev.2021.100641.

Li K R, Wang S Q, Cao M K. 2004. Vegetation and soil carbon storage in China. Science in China Series D-Earth Sciences, 47(1): 49–57.

Li P C, Chen J D, Li Y X, et al. 2023. Using the InVEST-PLUS model to predict and analyze the pattern of ecosystem carbon storage in Liaoning Province, China. Remote Sensing, 15(16): 4050, doi: 10.3390/rs15164050.

Li R, Shi Y, Feng C C, et al. 2021. The spatial relationship between ecosystem service scarcity value and urbanization from the perspective of heterogeneity in typical arid and semiarid regions of China. Ecological Indicators, 132: 108299, doi: 10.1016/j.ecolind.2021.108299.

Li S, Gu Y W, Chen J P. 2016. Spatio-temporal dynamical changes of land use in Ningxia Yellow River Valley. Journal of Southwest University (Natural Science Edition), 38(4): 42–49. (in Chinese)

Li W, Liu Y J, Yang Z F. 2012. Preliminary strategic environmental assessment of the Great Western Development Strategy: safeguarding ecological security for a new western China. Environmental Management, 49(2): 483–501.

Liang X, Guan Q F, Clarke K C, et al. 2021a. Understanding the drivers of sustainable land expansion using a patch-generating land use simulation (PLUS) model: A case study in Wuhan, China. Computers, Environment and Urban Systems, 85: 101569, doi: 10.1016/j.compenvurbsys.2020.101569.

Liang Y J, Hashimoto S, Liu L J. 2021b. Integrated assessment of land-use/land-cover dynamics on carbon storage services in the Loess Plateau of China from 1995 to 2050. Ecological Indicators, 120: 106939, doi: 10.1016/j.ecolind.2020.106939.

Liu Q, Yang D D, Cao L, et al. 2022. Assessment and prediction of carbon storage based on land use/land cover dynamics in the tropics: A case study of Hainan Island, China. Land, 11(2): 244, doi: 10.3390/land11020244.

Liu X P, Liang X, Li X, et al. 2017. A future land use simulation model (FLUS) for simulating multiple land use scenarios by coupling human and natural effects. Landscape and Urban Planning, 168: 94–116.

Lu H L, Zhou L H, Chen Y, et al. 2017. Degree of coupling and coordination of eco-economic system and the influencing factors: a case study in Yanchi County, Ningxia Hui Autonomous Region, China. Journal of Arid Land, 9(3): 446–457.

Lu Y Y, Xu X L, Zhao J H, et al. 2022. Spatiotemporal evolution of mountainous ecosystem services in an arid region and its influencing factors: A case study of the Tianshan Mountains in Xinjiang. Land, 11(12): 2164, doi: 10.3390/land11122164.

Lyu R F, Clarke K C, Zhang J M, et al. 2019. The impact of urbanization and climate change on ecosystem services: A case study of the city belt along the Yellow River in Ningxia, China. Computers, Environment and Urban Systems, 77: 101351, doi: 10.1016/j.compenvurbsys.2019.101351.

Maestre F T, Cortina J. 2004. Do positive interactions increase with abiotic stress? A test from a semi-arid steppe. Proceedings of the Royal Society B: Biological Sciences, 271(Suppl. 5): S331–S333.

Meentemeyer R K, Tang W W, Dorning M A, et al. 2013. FUTURES: multilevel simulations of emerging urban–rural landscape structure using a stochastic patch-growing algorithm. Annals of the Association of American Geographers, 103(4): 785–807.

Nie X, Lu B, Chen Z P, et al. 2020. Increase or decrease? Integrating the CLUMondo and InVEST models to assess the impact of the implementation of the Major Function Oriented Zone planning on carbon storage. Ecological Indicators, 118: 106708, doi: 10.1016/j.ecolind.2020.106708.

Piyathilake I D U H, Udayakumara E P N, Ranaweera L V, et al. 2022. Modeling predictive assessment of carbon storage using InVEST model in Uva Province, Sri Lanka. Modeling Earth Systems and Environment, 8(2): 2213–2223.

Posner S, Verutes G, Koh I, et al. 2016. Global use of ecosystem service models. Ecosystem Services, 17: 131–141.

Raich J W, Schlesinger W H. 1992. The global carbon dioxide flux in soil respiration and its relationship to vegetation and climate. Tellus B: Chemical and Physical Meteorology, 44(2): 81–99.

Sohl T L, Claggett P R. 2013. Clarity versus complexity: Land-use modeling as a practical tool for decision-makers. Journal of Environmental Management, 129: 235–243.

Song C, Yu Q Y, Wang R X. 2021. Spatio-temporal varaiation of windbreak and sand fixation functions based on vegetation coverage in Baijitan Nature Reserve, Ningxia. Acta Ecological Sinica, 41(8): 3131–3143. (in Chinese)

Tang X L, Zhao X, Bai Y F, et al. 2018. Carbon pools in China's terrestrial ecosystems: New estimates based on an intensive field survey. Proceedings of the National Academy of Sciences, 115(16): 4021–4026.

Verburg P H, Soepboer W, Veldkamp A, et al. 2002. Modeling the spatial dynamics of regional land use: the CLUE-S model. Environmental Management, 30(3): 391–405.

Wang C W, Luo J J, Qing F, et al. 2022a. Analysis of the driving force of spatial and temporal differentiation of carbon storage in Taihang Mountains based on InVEST model. Applied Sciences, 12(20): 10662, doi: 10.3390/app122010662.

Wang C Y, Li T Z, Guo X H, et al. 2022b. Plus-InVEST Study of the Chengdu-Chongqing urban agglomeration's land-use change and carbon storage. Land, 11(10): 1617, doi: 10.3390/land11101617.

Wang J F, Xu C D. 2017. Geodetector: Principle and prospective. Acta Geographica Sinica, 72(1): 116–134. (in Chinese)

Wang L, Du L T, Dan Y, et al. 2020. Carbon dynamic simulation of desert steppe ecosystem in different climate scenarios. Acta Ecologica Sinica, 40(2): 657–666. (in Chinese)

Wang P Q, Li R J, Liu D J, et al. 2022c. Dynamic characteristics and responses of ecosystem services under land use/land cover change scenarios in the Huangshui River Basin, China. Ecological Indicators, 144: 109539, doi: 10.1016/j.ecolind.2022.109539.

Wang Z Y, Li X, Mao Y T, et al. 2022d. Dynamic simulation of land use change and assessment of carbon storage based on climate change scenarios at the city level: A case study of Bortala, China. Ecological Indicators, 134: 108499, doi: 10.1016/j.ecolind.2021.108499.

Wei P J, Chen S Y, Wu M H, et al. 2021. Increased ecosystem carbon storage between 2001 and 2019 in the northeastern margin of the Qinghai-Tibet Plateau. Remote Sensing, 13(19): 3986, doi: 10.3390/rs13193986.

Wiesmeier M, von Lützow M, Spörlein P, et al. 2015. Land use effects on organic carbon storage in soils of Bavaria: the importance of soil types. Soil and Tillage Research, 146: 296–302.

Wu D, Li H, Ai N, et al. 2020. Predicting spatiotemporal changes in land use and habitat quality based on CA-Markov: A case study in central Ningxia, China. Chinese Journal of Eco-Agriculture, 28(12): 1969–1978.

Xiang M S, Wang C J, Tan Y X, et al. 2022. Spatio-temporal evolution and driving factors of carbon storage in the Western Sichuan Plateau. Scientific Reports, 12(1): 8114, doi: 10.1038/s41598-022-12175-8.

Xie X L, Sun B, Zhou H Z, et al. 2004. Soil carbon stocks and their influencing factors under native vegetations in China. Acta Pedologica Sinica, 41(5): 687–699. (in Chinese)

Xu L, Yu G R, He N P, et al. 2018. Carbon storage in China's terrestrial ecosystems: A synthesis. Scientific Reports, 8: 2806, doi: 10.1038/s41598-018-20764-9.

Xu L, He N P, Yu G R. 2019. A dataset of carbon density in Chinese terrestrial ecosystems (2010s). China Scientific Data, 4(1): 90–96. (in Chinese)

Xu L F, Liu X, Tong D, et al. 2022. Forecasting urban land use change based on cellular automata and the PLUS model. Land,

11(5): 652, doi: 10.3390/land11050652.

Xu X M, Du Z Q, Zhang H. 2016. Integrating the system dynamic and cellular automata models to predict land use and land cover change. International Journal of Applied Earth Observation and Geoinformation, 52: 568–579.

Yang F X, Yang M, Xue B, et al. 2018. The effects of China's western development strategy implementation on local ecological economic performance. Journal of Cleaner Production, 202: 925–933.

Yang J, Xie B P, Zhang D G. 2021. Spatio-temporal evolution of carbon stocks in the Yellow River Basin based on InVEST and CA-Markov models. Chinese Journal of Eco-Agriculture, 29(6): 1018–1029.

Yang L W, Wang D Y. 2009. Evaluation of ecological service value of wind-break and sand-fixation function of Shapotou sand-binding vegetation ecosystem. Journal of Shanxi Normal University (Natural Science Edition), 23(4): 94–98. (in Chinese)

Zhang P P, Li Y H, Yin H R, et al. 2022a. Spatio-temporal variation and dynamic simulation of ecosystem carbon storage in the north-south transitional zone of China. Journal of Natural Resources, 37(5): 1183–1197. (in Chinese)

Zhang S R, Bai X Y, Zhao C W, et al. 2022b. China's carbon budget inventory from 1997 to 2017 and its challenges to achieving carbon neutral strategies. Journal of Cleaner Production, 347: 130966, doi: 10.1016/j.jclepro.2022.130966.

Zhao M M, He Z B, Du J, et al. 2019. Assessing the effects of ecological engineering on carbon storage by linking the CA-Markov and InVEST models. Ecological Indicators, 98: 29–38.

Zhao Z Q, Sharifi A, Dong X, et al. 2021. Spatial variability and temporal heterogeneity of surface urban heat island patterns and the suitability of local climate zones for land surface temperature characterization. Remote Sensing, 13(21): 4338, doi: 10.3390/rs13214338.

Zhu L Y, Hu K, Sun S, et al. 2022. Research on the spatiotemporal variation of carbon storage in the coastal zone of Liaoning Province based on InVEST model. Geoscience, 36(1): 96–104. (in Chinese)

Zhu W B, Zhang J J, Cui Y P, et al. 2019. Assessment of territorial ecosystem carbon storage based on land use change scenario: A case study in Qihe River Basin. Acta Geographica Sinica, 74(3): 446–459. (in Chinese)

Appendix

1 Land expansion analysis strategy

By overlaying two-period land use data (1990 and 2020) and extracting cells with changed status from the later date land use data (2020), we obtained the land expansion map for each land use type. The development probability of each land use type was calculated using a random forest (RF) algorithm, and the contribution of various factors driving the land expansion was evaluated using the specific formula (Eq. S1) on the basis of two-period land use data (Xu et al., 2022):

$$P_{i,k}^{d}(x)=\frac{\sum_{n=1}^{M} I(h_n(x)=d)}{M}, \tag{S1}$$

where $P_{i,k}^{d}(x)$ is the development probability of land use type k at grid cell i; the value of d is either 0 or 1 (the value of 1 indicates that there are other land use types that change to land use type k, while the value of 0 represents other transitions); x is a vector that consists of multiple driving factors; M is the total count of decision trees; I is the indicative function of the decision tree set; and $h_n(x)$ is the prediction type of the n^{th} decision tree (n=1, 2, …, M) for vector x. In addition, the RF algorithm has the advantage of measuring the importance of independent variables to the variation of dependent variables, which can be calculated according to the variation of the out-of-bag error caused by stochastic noise.

2 Cellular automata (CA) model based on multi-type random patch seeds

The generation of land use patches was simulated within the bounds of the development probability for each land use type based on a combination of random seed generation and a threshold decreasing mechanism (Wang et al., 2022b). Neighborhood weight parameter was obtained by computing the ratio of the expansion area of a given land use type to the total area of the given land use type based on the land expansion map (Table S1) (Wang et al, 2019; Li et al., 2021). The land use transfer cost matrix of the Ningxia Section of Yellow River Basin (NYRB) (Table S2) was obtained using the land use transfer matrix from 1990 to 2020.

Table S1 Neighborhood weight parameter of each land use type under the four land use scenarios

Land use scenario	Neighborhood weight parameter					
	Cultivated land	Woodland	Grassland	Water body	Unused land	Construction land
NDS	0.0622	0.2498	0.0850	0.1654	0.0028	0.7429
EPS	0.0438	0.4268	0.0850	0.2806	0.0578	0.2743
UDS	0.0987	0.2498	0.0850	0.1654	0.0028	1.0000
CPS	0.0992	0.3383	0.1980	0.1654	0.0578	0.7429

Note: NDS, natural development scenario; EPS, ecological protection scenario; UDS, urban development scenario; CPS, cultivated land protection scenario.

Table S2 Land use transfer cost matrix of the Ningxia Section of Yellow River Basin (NYRB)

Land use scenario	Land use type	Cultivated land	Woodland	Grassland	Water body	Unused land	Construction land
NDS	Cultivated land	1	0	1	1	1	1
	Woodland	0	1	0	0	0	0
	Grassland	1	1	1	1	1	1
	Water body	1	0	1	1	0	1
	Unused land	1	0	1	1	1	1
	Construction land	0	0	0	1	0	1

To be continued

Continued

Land use scenario	Land use type	Cultivated land	Woodland	Grassland	Water body	Unused land	Construction land
EPS	Cultivated land	1	0	1	1	1	1
	Woodland	0	1	0	0	0	0
	Grassland	1	1	1	1	0	0
	Water body	0	0	1	1	0	0
	Unused land	1	0	1	1	1	1
	Construction land	0	0	0	1	0	1
UDS	Cultivated land	1	0	1	1	1	1
	Woodland	0	1	0	0	0	0
	Grassland	1	1	1	1	1	1
	Water body	1	0	1	1	0	1
	Unused land	1	0	1	1	1	1
	Construction land	0	0	0	0	0	1
CPS	Cultivated land	1	0	0	0	0	0
	Woodland	0	1	0	0	0	0
	Grassland	1	1	1	1	1	1
	Water body	1	0	1	1	0	1
	Unused land	1	0	1	1	1	1
	Construction land	1	0	0	1	0	1

Note: "0" means that there is no conversion between two land use types and "1" indicates that the conversion is allowed between two land use types.

References

Li C, Wu Y M, Gao B P, et al. 2021. Multi-scenario simulation of ecosystem service value for optimization of land use in the Sichuan-Yunnan ecological barrier, China. Ecological Indicators, 132: 108328, doi: 10.1016/j.ecolind.2021.108328.

Wang B S, Liao J F, Zhu W, et al. 2019. The weight of neighborhood setting of the FLUS model based on a historical scenario: A case study of land use simulation of urban agglomeration of the Golden Triangle of Southern Fujian in 2030. Acta Ecologica Sinica, 39: 4284–4298. (in Chinese)

Wang C Y, Li T Z, Guo X H, et al. 2022. Plus-InVEST study of the Chengdu-Chongqing urban agglomeration's land-use change and carbon storage. Land, 11(10): 1617, doi: 10.3390/land11101617.

Xu L F, Liu X, Tong D, et al. 2022. Forecasting urban land use change based on cellular automata and the PLUS model. Land, 11(5): 652, doi: 10.3390/land11050652.